



FULL PAPER

Green synthesis of 1*H*-pyrazolo[1,2-*b*]phthalazine-2-carbonitrile derivatives using a new bifunctional base–ionic liquid hybrid magnetic nanocatalyst

Mahdia Hamidinasab^{1,2} | Mohammad Ali Bodaghifard^{1,2} | Akbar Mobinikhalevi^{1,2}

¹ Department of Chemistry, Faculty of Science, Arak University, Arak 38156-88138, Iran

² Institute of Nanosciences and Nanotechnology, Arak University, Arak 38156-88138, Iran

Correspondence

Mahdia Hamidinasab and Mohammad Ali Bodaghifard, Department of Chemistry, Faculty of Science, Arak University, Arak 38156-88138, Iran.

Email: mahdiahaminasab@yahoo.com; mbodaghi2007@yahoo.com

The ionic liquid-base *N,N*,2,2,6,6-hexamethyl-*N*-(3-(trimethoxysilyl)propyl)piperidin-4-amonium iodide was grafted onto titana-coated NiFe₂O₄ nanoparticles for obtaining an efficient and reusable ionic liquid-base hybrid nanocatalyst. The structure of hybrid nanoparticles was characterized using FT-IR (Fourier-transform infrared spectroscopy), field emission scanning electron microscopy, EDS (energy-dispersive X-ray spectroscopy), EDS map scan, Brunauer–Emmett–Teller surface area analysis, CHN (elemental analysis), vibrating sample magnetometer and thermogravimetric analysis techniques. Furthermore, this novel hybrid catalyst was used in one-pot three-component synthesis of 3-amino-1-aryl-5,10-dioxo-1*H*-pyrazolo[1,2-*b*]phthalazine-2-carbonitrile derivatives under green and environmentally benign conditions. This protocol avoids the use of harmful catalysts, toxic solvents and harsh reaction conditions. The products were synthesized in excellent yields within short reaction time and identified using elemental analysis, FT-IR, ¹H NMR and ¹³C NMR spectroscopies.

KEYWORDS

ionic liquid, hybrid nanostructures, heterogeneous catalysis, green synthesis, phthalazine-dione

1 | INTRODUCTION

Heterocyclic compounds containing two active pharmacophores including fused pyrazolo and phthalazine moieties have properties such as anticancer,^[1–3] anticonvulsant,^[4] antiflammatory^[5] and antimicrobial activity.^[6,7]

Multicomponent reactions (MCRs), in which three or more different compounds react to give a single product (so-called domino), are one of the most convenient and cost-effective synthesis methods for preparation of vital and pharmaceutically important heterocyclic compounds. As a result, MCRs cut the reaction time and simplify purification.

Nanocatalysis is a developed field in green chemistry which involves the use of nanoscale materials as homogeneous and heterogeneous catalysts for a variety of

chemical reactions.^[8–14] The use of magnetic nanoparticles (MNPs) has attracted particular interest in chemical reactions owing to their super-paramagnetic behavior and easy separation from the reaction media, large surface area, low toxicity, good stability and possible functionalization.^[10,14] However, the magnetic nanoparticles are unstable over longer periods of time and tend to aggregate into large clusters. Encapsulation of magnetic nanoparticles with a suitable passive material or porous materials such as polymer, silica and titana is an effective way to improve their chemical stability and prevent their aggregations.^[11–15]

From the initial use of ionic liquids (ILs), which are made up of cationic and anionic components, they have found applications in various fields such as environmentally friendly solvents and catalysis. Ionic liquids are capable of restricting many of the negative effects of the

conventional organic solvents or other catalysts during catalytic reactions and have successfully been used in various catalytic areas affording high catalytic activity.^[16] Unfortunately, the difficulty of their recovery and extreme viscosity have restrained their application in catalytic reactions.^[17,18] Therefore, the heterogenization of ILs on appropriate porous carriers or suitable magnetic nanoparticles would be a viable and appealing approach to fabricate an efficient solid catalyst with superior activity and stability.^[11–14,19] Furthermore, heterogenized ILs on magnetic nanoparticles have found remarkable applications, such as adsorbents for magnetic solid-phase extraction of sulfonylurea herbicides,^[20] adsorbents for magnetic dispersive solid-phase extraction of cephalosporins^[21] and removal of anionic dye from water.^[22]

Based on the above considerations, the main purpose of this research is the preparation of a hybrid magnetic nanostructure (MNPs@TiO₂–ILPip) with both basic and ionic liquid counterparts, allowing the favorable combination of their properties. To develop the green procedures for the synthesis of valuable heterocyclic compounds, herein an environmentally benign protocol is investigated for the synthesis of some phthalazine-trione derivatives,^[23–25] via the three-component reaction of phthalhydrazide, malononitrile and aldehydes (Scheme 1) in the presence of ionic liquid base grafted onto TiO₂-coated nickel-ferrite nanoparticles

(nano-NiFe₂O₄@TiO₂–ILPip) as an efficient hybrid nanocatalyst under green conditions.

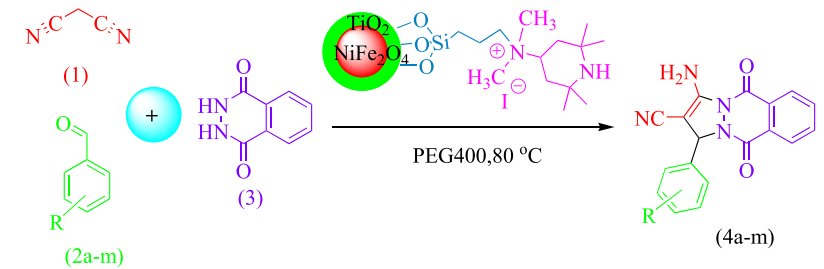
2 | RESULTS AND DISCUSSION

In this study, ionic liquid-base tag was grafted onto nickel ferrite nanoparticles for the preparation of an efficient and heterogeneous magnetic nanocatalyst. We found that these nanoparticles act as an effective hybrid catalyst in the synthesis of biologically active phthalazine-trione derivatives.

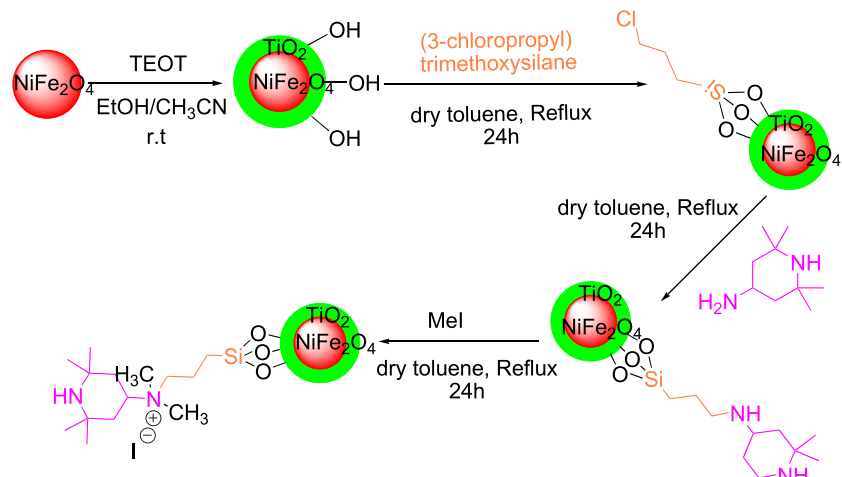
2.1 | Preparation and characterization of novel nano-NiFe₂O₄@TiO₂–ILPip as a catalyst

The schematic preparation of MNPs@TiO₂–ILPip is presented in Scheme 2. The prepared catalyst was characterized by various standard techniques, including Fourier transform infrared (FT-IR) spectroscopy, field emission scanning electron microscopy (FE-SEM), energy dispersive X-ray spectroscopy (EDS), EDS map scan, vibrating sample magnetometer (VSM), X-ray powder diffraction (XRD), thermogravimetric analysis (TGA) and Brunauer–Emmett–Teller surface area analysis (BET).

SCHEME 1 The synthetic pathway for preparation of 3-amino-1-aryl-5,10-dioxo-1*H*-pyrazolo[1,2-*b*]phthalazine-2-carbonitrile derivatives in the presence of nano-NiFe₂O₄@TiO₂–ILPip particles



SCHEME 2 Preparation of hybrid MNPs@TiO₂–ILPip



The FT-IR spectra of bare NiFe_2O_4 MNPs, $\text{NiFe}_2\text{O}_4@\text{TiO}_2$ MNPs, nano- $\text{NiFe}_2\text{O}_4@\text{TiO}_2\text{-PrCl}$, nano- $\text{NiFe}_2\text{O}_4@\text{TiO}_2\text{-4APip}$ and nano- $\text{NiFe}_2\text{O}_4@\text{TiO}_2\text{-ILPip}$ that were recorded in the range of 400–4000 cm^{-1} are shown in Figure 1. As can be seen in curve (a), the spectrum of NiFe_2O_4 nanoparticles shows strong absorption bands around 401 and 601 cm^{-1} corresponding to the

stretching vibration of metal at octahedral M–O and tetrahedral M–O sites.^[26] The weak absorption bands at 1400 and 798 cm^{-1} in curves b–e are assigned to the stretching vibration of Ti–O–Ti.^[27,28] The weak band at 1644 cm^{-1} and the broad band in the range of 3200–3600 cm^{-1} are due to twisting vibration mode of H–O–H adsorbed in the titana shell and stretching vibra-

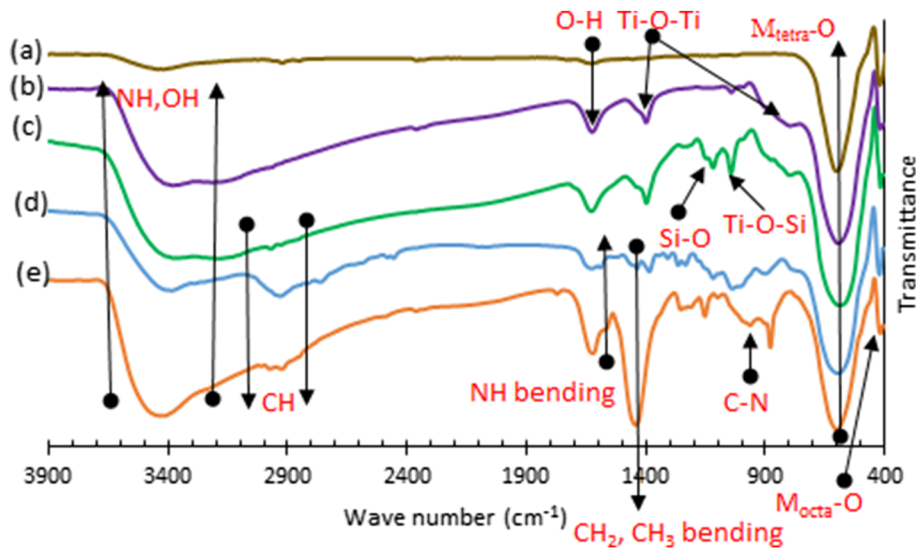
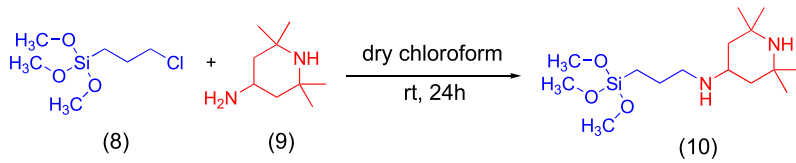


FIGURE 1 The Fourier-transform infrared spectroscopy (FT-IR) spectra of (a) nano- NiFe_2O_4 , (b) nano- $\text{NiFe}_2\text{O}_4@\text{TiO}_2$, (c) nano- $\text{NiFe}_2\text{O}_4@\text{TiO}_2\text{-PrCl}$, (d) nano- $\text{NiFe}_2\text{O}_4@\text{TiO}_2\text{-4APip}$ and (e) nano- $\text{NiFe}_2\text{O}_4@\text{TiO}_2\text{-ILPip}$.



SCHEME 3 Preparation of 2,2,6,6-tetramethyl-N-[3-(trimethoxysilyl)propyl]piperidin-4-amine

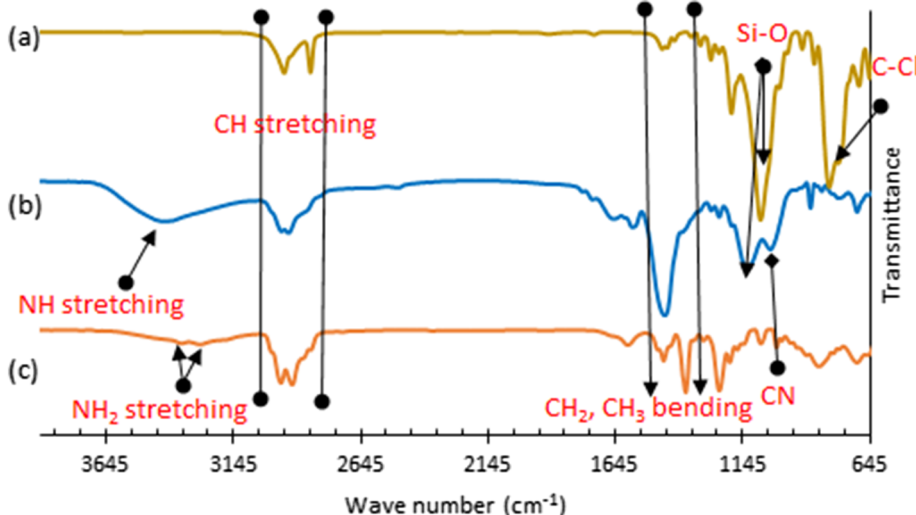


FIGURE 2 The FT-IR spectra of (a) (3-chloropropyl)trimethoxysilane, (b) 2,2,6,6-tetramethyl-N-(3-(trimethoxysilyl)propyl)piperidin-4-amine and (c) 2,2,6,6-tetramethylpiperidin-4-amine.

tion mode of Ti–O, respectively. The presence of the anchored alkyl groups is confirmed by the weak aliphatic C–H symmetric and asymmetric stretching vibrations at 2920 and 2977 cm⁻¹ and bending vibrations around

1400 cm⁻¹ (curves c–e). In curve e, the strong bending band at 1444 cm⁻¹ is attributed to anchored CH₃ groups on the final MNPs catalyst. In curve c, absorption bonds at 1040 and 1122 cm⁻¹ correspond to the stretching

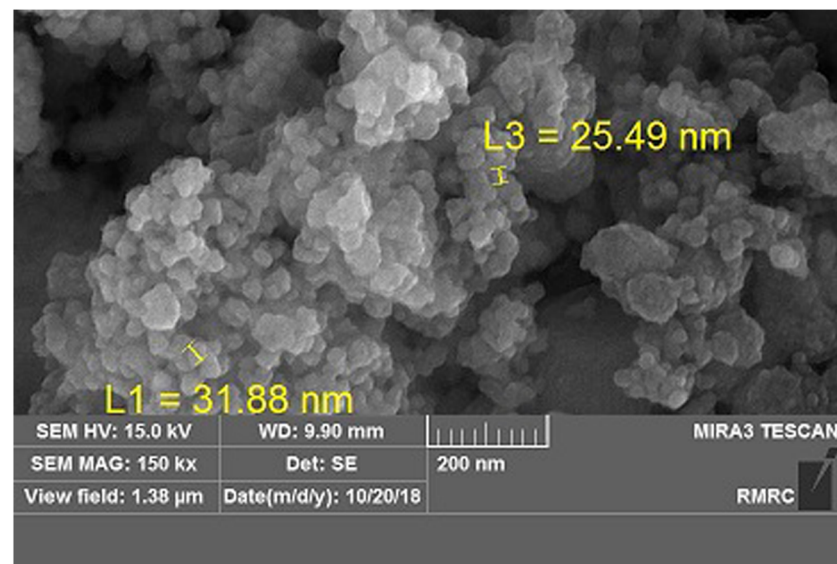


FIGURE 3 The field emission scanning electron microscopy (FE-SEM) image of nano-NiFe₂O₄@TiO₂-ILPip

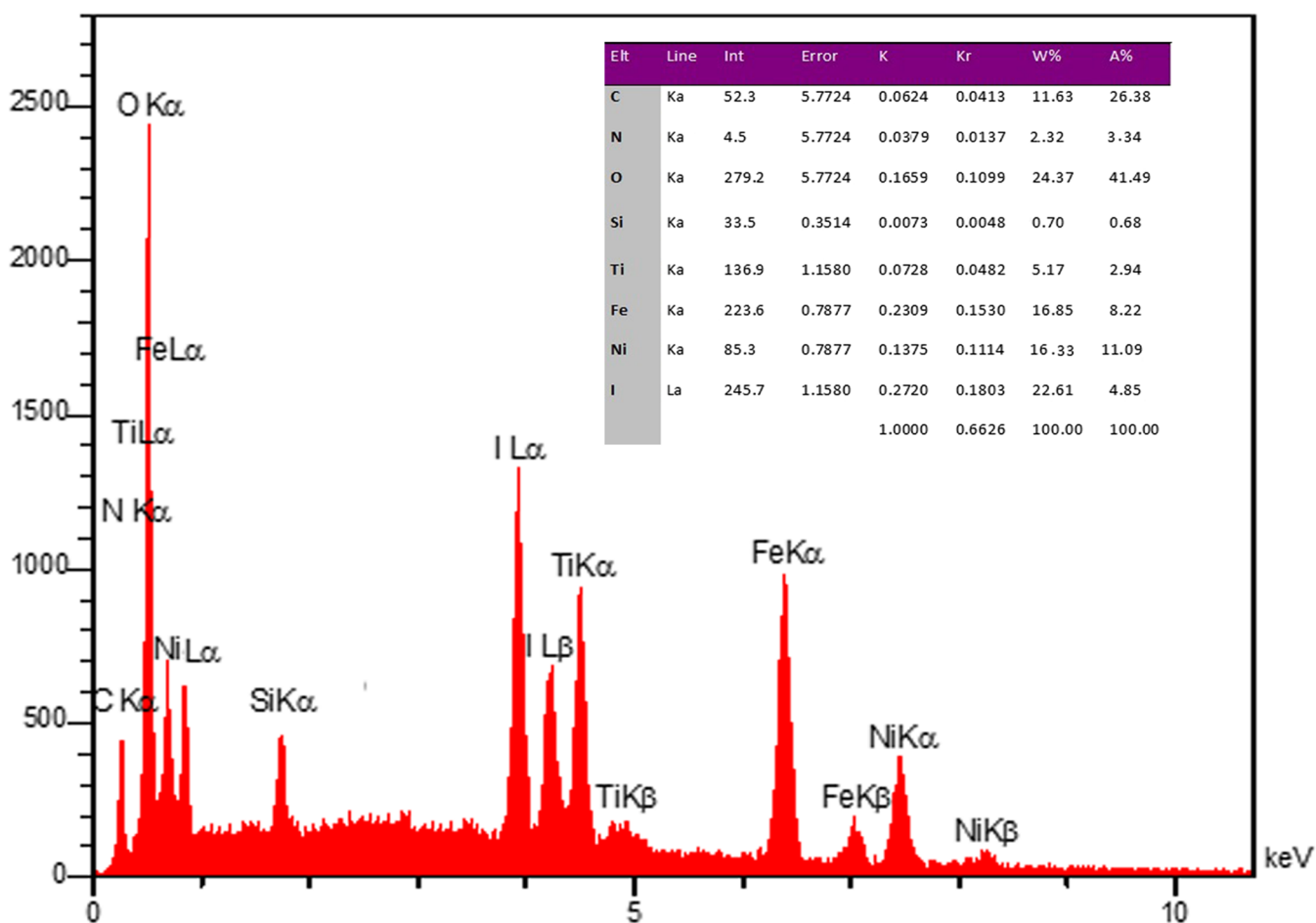


FIGURE 4 The energy-dispersive X-ray spectroscopy (EDS) spectrum of nano-NiFe₂O₄@TiO₂-ILPip particles

vibration of Ti–O–Si and Si–O, respectively.^[29,30] The NH bending and C–N stretching bands appear at 1591 and 1010 cm⁻¹ in curves d and e, respectively.

In order to prove the preparation of nano-NiFe₂O₄@TiO₂–4APip, and the existence of the tetramethylpiperidine group in this structure, the compound 2,2,6,6-tetramethyl-*N*-(3-(trimethoxysilyl)propyl)piperidin-4-amine was separately synthesized (Scheme 3).

The FT-IR spectra of (3-chloropropyl)trimethoxysilane, 2,2,6,6-tetramethyl-*N*-(3-(trimethoxysilyl)propyl)piperidin-4-amine and 2,2,6,6-tetramethylpiperidin-4-amine are presented in Figure 2. As shown in curve b, the NH₂ absorption bands at 3272 and 3346 cm⁻¹ (Figure 2, curve c) and C–Cl absorption band at 805 cm⁻¹ (Figure 2, curve a) are omitted and new stretching absorption bands appear at 3425 cm⁻¹ (NH) and 1100 cm⁻¹ (C–N). The results confirm the successful grafting of functional groups onto the surface of the prepared nanostructure.

Figure 3 shows the FE-SEM image of nano-NiFe₂O₄@TiO₂–ILPip nanostructure. The particles are almost

spherical with regular shape and have a mean diameter of about 34 nm.

Figure 4 shows the EDS of nano-NiFe₂O₄@TiO₂–ILPip particles. The presence of Fe, Ni, Ti, Si, N, C, O and I atoms in the EDs spectrum is shown. Also, the EDS map scan of nano-NiFe₂O₄@TiO₂–ILPip particles (Figure 5) shows the excellent dispersion of the present elements on the surface of the MNP catalyst. These

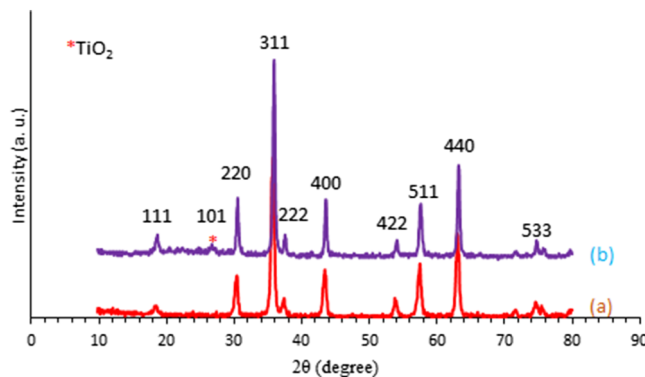


FIGURE 6 The XRD patterns of (a) NiFe₂O₄ nanoparticles and (b) nano-NiFe₂O₄@TiO₂–ILPip particles

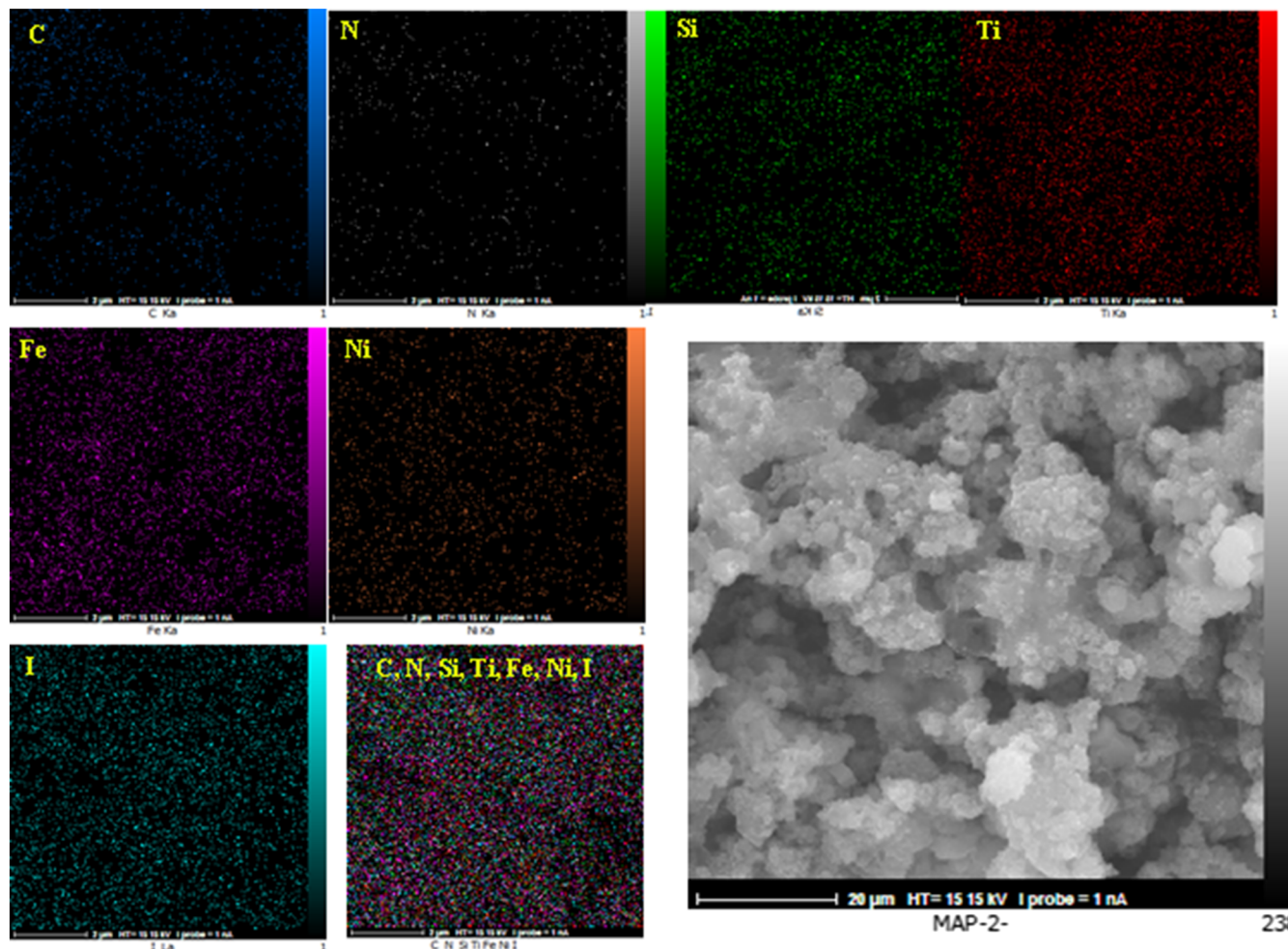


FIGURE 5 The EDS map scan of nano-NiFe₂O₄@TiO₂–ILPip particles

results confirm the successful formation of nano-NiFe₂O₄@TiO₂-ILPip catalyst.

The X-ray diffraction patterns of the synthesized NiFe₂O₄ nanoparticles and nano-NiFe₂O₄@TiO₂-ILPip particles are shown in Figure 6. Several diffraction peaks appeared at (111), (220), (311), (222), (400), (422), (511), (440) and (533) miller planes, which confirms the cubic crystal structure of NiFe₂O₄ nanoparticles^[31,32] and conforms with the JCPDS file (no. 44-1485) standard.^[26] The peak at $2\theta = 26.6^\circ$ indicates the formation of a TiO₂ layer in the structure of nano-NiFe₂O₄@TiO₂-ILPip particles (Figure 6b).^[31] The average size of the crystallites was calculated by applying Scherer's equation: $D = 0.9\lambda/\beta \cos \theta$, where h is the diffraction angle, λ is the wavelength of the incident X-rays, β is full width at half maximum height in radians, θ is the Bragg diffraction angle and D is the average diameter in Å. The peak at $2\theta = 35.7^\circ$ (311 plane) is selected to calculate the crystallite size. It

is found that the particle diameter is about 39 nm, which is in good agreement with FE-SEM analysis (Figure 3).

The TGA in Figure 7 shows the stability of the nano-NiFe₂O₄@TiO₂-ILPip catalyst. As shown, the initial 3% weight loss from room temperature to about 200°C, is due to the removal of physically adsorbed solvent and surface hydroxyl groups (Figure 7). The major weight loss (19%) beyond 200°C to nearly 700°C is attributed to the decomposition of the organic moieties within the nanocatalyst structure. Therefore, the catalyst shows reasonable stability up to 200°C and it is safe to carry out the reaction under heterogeneous conditions.

The magnetic properties of nanoparticles were characterized using a VSM (Figure 8). The typical room temperature magnetization curves a and b refer to NiFe₂O₄ MNPs and nano-NiFe₂O₄@TiO₂-ILPip. The hysteresis curve allows determination of the coercivity (H_c), remanent magnetization (M_r) and saturation magnetization (M_s).

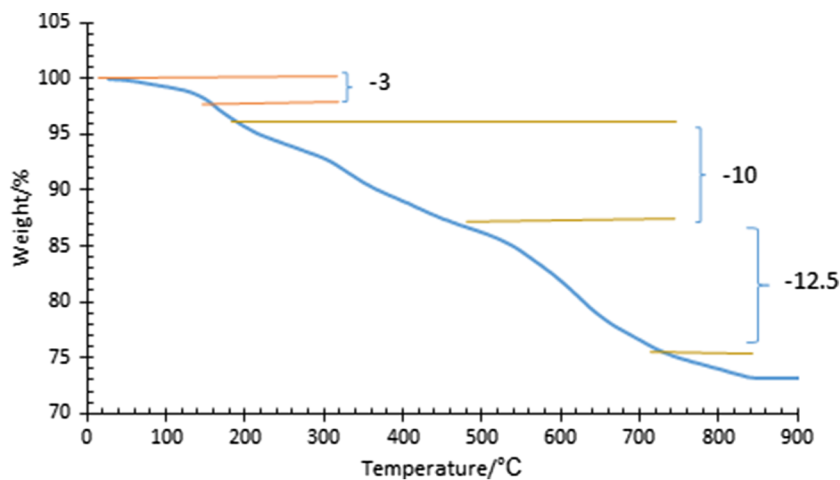


FIGURE 7 The thermogravimetric analysis (TGA) curve of nano-NiFe₂O₄@TiO₂-ILPip particles

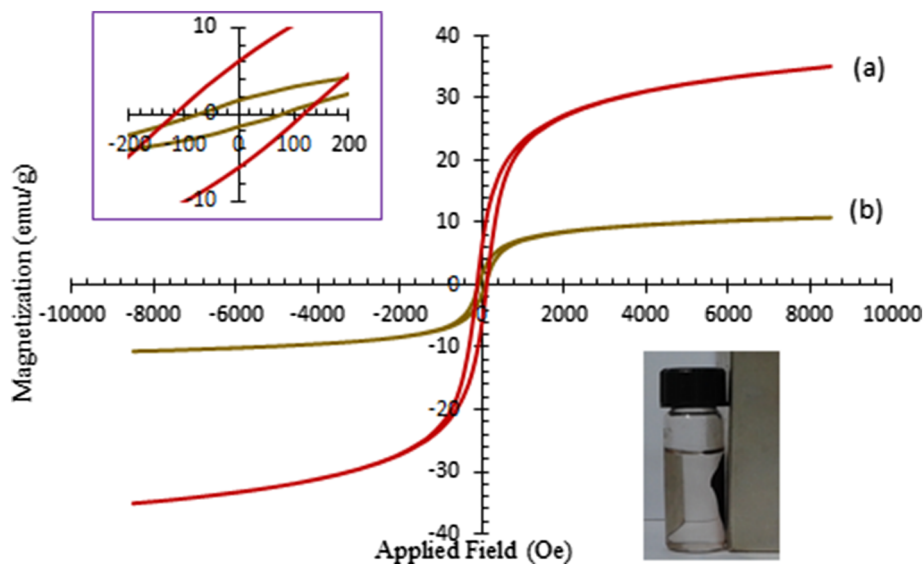


FIGURE 8 Magnetic hysteresis loops of (a) NiFe₂O₄ MNPs and (b) nano-NiFe₂O₄@TiO₂-ILPip particles

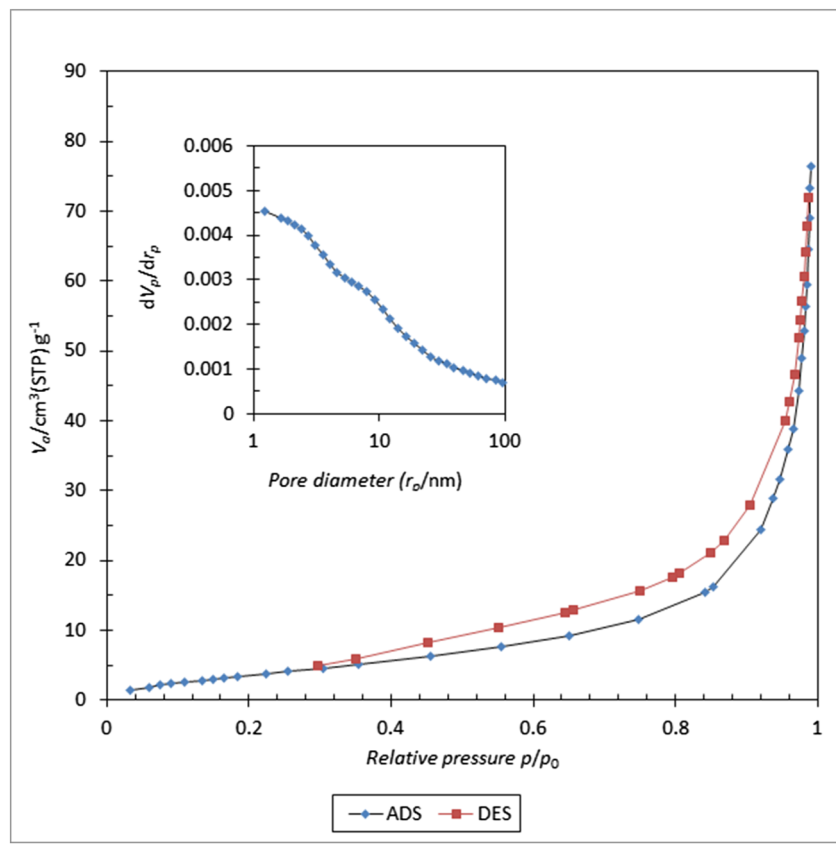


FIGURE 9 N_2 physisorption isotherms and pore size distribution (inset) of nano- $\text{NiFe}_2\text{O}_4@\text{TiO}_2$ -ILPip particles

TABLE 1 The optimization of reaction conditions for synthesis of 3-amino-1-aryl-5,10-dioxo-1H-pyrazolo[1,2-b]phthalazine-2-carbonitrile derivatives ^a

Entry	Catalyst (mg)	Solvent	Temperature (°C)	Time	Yield (%) ^b
1	PTSA (20)	EtOH	Reflux	24 h	30
2	Piperidine (20)	EtOH	Reflux	8 h	76
3	2,2,6,6-Tetramethyl-4-amino piperidine (20)	EtOH	Reflux	6 h	86
4	Nano- $\text{NiFe}_2\text{O}_4@\text{TiO}_2$ -ILPip (10)	EtOH	Reflux	2.5 h	89
5	Nano- $\text{NiFe}_2\text{O}_4@\text{TiO}_2$ -ILPip (10)	CHCl_3	Reflux	24 h	80
6	Nano- $\text{NiFe}_2\text{O}_4@\text{TiO}_2$ -ILPip (10)	H_2O	Reflux	10 h	75
7	Nano- $\text{NiFe}_2\text{O}_4@\text{TiO}_2$ -ILPip (10)	Toluene	Reflux	24 h	46
8	Nano- $\text{NiFe}_2\text{O}_4@\text{TiO}_2$ -ILPip (10)	No solvent	Room temperature	24 h	80
9	Nano- $\text{NiFe}_2\text{O}_4@\text{TiO}_2$ -ILPip (10)	No solvent	70	14 h	85
10	Nano- $\text{NiFe}_2\text{O}_4@\text{TiO}_2$ -ILPip (10)	No solvent	100	10 h	85
11	Nano- $\text{NiFe}_2\text{O}_4@\text{TiO}_2$ -ILPip (10)	PEG 400	70	1.5 h	75
12	Nano- $\text{NiFe}_2\text{O}_4@\text{TiO}_2$ -ILPip (10)	PEG 400	90	30 min	85
13	Nano- $\text{NiFe}_2\text{O}_4@\text{TiO}_2$ -ILPip (10)	PEG 400	110	30 min	85
14	Nano-$\text{NiFe}_2\text{O}_4@\text{TiO}_2$-ILPip (20)	PEG 400	90	10 min	97
15	Nano- $\text{NiFe}_2\text{O}_4@\text{TiO}_2$ -ILPip (30)	PEG 400	90	10 min	96
16	Nano- $\text{NiFe}_2\text{O}_4@\text{TiO}_2$ -4-APip (20)	PEG 400	90	45 min	90
17	NiFe_2O_4 (20)	PEG 400	90	4 h	70
18	No catalyst	PEG 400	90	7 h	53
19	No catalyst	EtOH	Reflux	24 h	30

Note. The bold entry is for optimized reaction condition.

^aReaction conditions: malononitrile, 1.5 mmol; phthalhydrazide, 1 mmol; 4-chlorobenzaldehyde, 1 mmol; and nanocatalyst.

^bIsolated yield.

The magnetization of sample could be completely saturated at high fields of up to ± 8000.0 Oe and the M_s of samples changes from 35.1 to 10.8 emu g⁻¹ owing to the formation of nano-NiFe₂O₄@TiO₂-ILPip catalyst. The hysteresis loops show the super paramagnetic behavior of the NiFe₂O₄ and NiFe₂O₄@TiO₂-ILPip particles in which M_r and H_c are close to zero ($M_r = 119$ and 80 emu g⁻¹ and $H_c = 6.1$ and 1.5 Oe, respectively).^[33]

The surface area of the prepared nanostructure was achieved by BET analysis. N₂ adsorption-desorption isotherms of nano-NiFe₂O₄@TiO₂-ILPip particles are shown in Figure 9. The pore size distribution plot is shown as an inset in the respective isotherm. The nano-NiFe₂O₄@TiO₂-ILPip particles exhibited type IV adsorption-desorption isotherm with an elongated S-type hysteresis loop. The specific surface area (a_s) 15.02 m²/g and total pore volume ($\rho/\rho^\circ = 0.990$) 0.115 cm³/g were observed.

2.2 | Synthesis of 3-amino-1-aryl-5,10-dioxo-1*H*-pyrazolo[1,2-*b*]phthalazine-2-carbonitrile derivatives

After characterization of the prepared hybrid nanostructure, its role as a catalyst was evaluated for synthesis of 3-amino-1-aryl-5,10-dioxo-1*H*-pyrazolo[1,2-*b*]phthalazine-2-carbonitriles **4a-m** (Scheme 1). The one-pot three-component condensation reaction of malononitrile (**1**, 1.5 mmol), 4-chlorobenzaldehyde (**2 g**, 1 mmol) and phthalhydrazide (**3**, 1 mmol) as a model

reaction to synthesize the desired product was tested (Table 1). The basic catalysts are superior to acidic catalysts (Table 1, entries 1-3).

The model reaction was carried out in several solvents such as CHCl₃, EtOH, toluene, PEG400 and H₂O under reflux and also under solvent-free conditions in the presence of IL-based nanocatalyst (Table 1). As shown in Table 1, it was found that conventional heating at 90°C and the use of PEG400 as a green solvent is more efficient than other conditions (Table 1, entry 12). The different amounts of IL-based nanocatalysts were loaded in the model reaction. The optimal amount of catalyst was 20 mg (Table 1, entry 14). To define the role and performance of IL-based nanocatalyst, the model reaction was carried out with 2,2,6,6-tetramethyl-4-amino piperidine, NiFe₂O₄ and nano-NiFe₂O₄@TiO₂-ILPip, nano-NiFe₂O₄@TiO₂-4-APip and without the catalyst (Table 1, entries 3 and 16-19). With respect to product yield and reaction time, the best result was obtained using nano-NiFe₂O₄@TiO₂-ILPip as a hybrid nanocatalyst (Table 1, Entry 14).

With optimized conditions in hand, the scope and limitation of this method were investigated for the desired product synthesis. The different aromatic aldehydes with electron-donating and electron-withdrawing substituents (**2a-m**) were reacted with phthalhydrazide (**3**) and malononitrile (**1**) to give the corresponding 3-amino-1-aryl-5,10-dioxo-1*H*-pyrazolo[1,2-*b*] phthalazine-2-carbonitrile derivatives (**4a-m**) with good to excellent yields (Table 2). To prove the benefits of prepared hybrid catalysts such as simple conditions and excellent yields in short reaction times, we compared its efficiency with that

TABLE 2 The synthesis of 3-amino-1-aryl-5,10-dioxo-1*H*-pyrazolo[1,2-*b*]phthalazine-2-carbonitrile derivatives using nano-NiFe₂O₄@TiO₂-ILPip^a

Entry	Aldehyde	Product	Time (min)	Yield (%) ^b	M.p (°C), with reference
1	3-Nitrobenzaldehyde	4a	35	93	265 ^[34]
2	4-Nitrobenzaldehyde	4b	45	95	258 ^[35]
3	3-Nitro-4-hydroxy-benzaldehyde	4c	35	93	259
4	Benzaldehyde	4d	30	95	265 ^[34]
5	2-Chlorobenzaldehyde	4e	25	93	252 ^[34]
6	3-Chlorobenzaldehyde	4f	25	95	267 ^[36]
7	4-Chlorobenzaldehyde	4g	10	97	270 ^[34]
8	2,4-Dichlorobenzaldehyde	4h	15	95	255 ^[37]
9	4-Bromobenzaldehyde	4i	15	96	269 ^[34]
10	2-Methoxybenzaldehyde	4j	45	89	255 ^[38]
11	3-Methoxybenzaldehyde	4k	45	85	265 ^[36]
12	4-Methoxybenzaldehyde	4l	60	90	247 ^[34]
13	3,4-Dimethoxybenzaldehyde	4m	70	85	235 ^[36]

^aReaction conditions: malononitrile, 1.5 mmol; phthalhydrazide, 1 mmol; 4-dichlorobenzaldehyde, 1 mmol; and nanocatalyst, 20 mg.

^bIsolated yield.

of other reported catalysts for synthesis of 3-amino-1-aryl-5,10-dioxo-1*H*-pyrazolo[1,2-*b*]phthalazine-2-carbonitrile derivatives in the literature (Table 3). As can be seen, this hybrid nanocatalyst is superior to other catalysts.

The proposed mechanism of the reaction is illustrated in Scheme 4. As the initiation step, malononitrile (**1**) gives malononitryl anion (**1'**) assisted by base moiety of catalyst and the carbonyl group activated by coordination with the ionic moiety of the catalyst (Scheme 4). Then the arylidenemalononitrile intermediate (**2'**) formed by

standard Knoevenagel condensation of malononitrile anion and aldehyde (**2**). The subsequent Michael-type addition of phthalhydrazide (**3**) to the intermediate (**2'**), followed by cyclization (**3'**) and tautomerization (**4'**), affords the corresponding products (**4**).^[38,44]

2.3 | Catalyst recovery and reusability

To investigate the recovery and recyclability of the catalyst for green chemistry and commercial applications, the

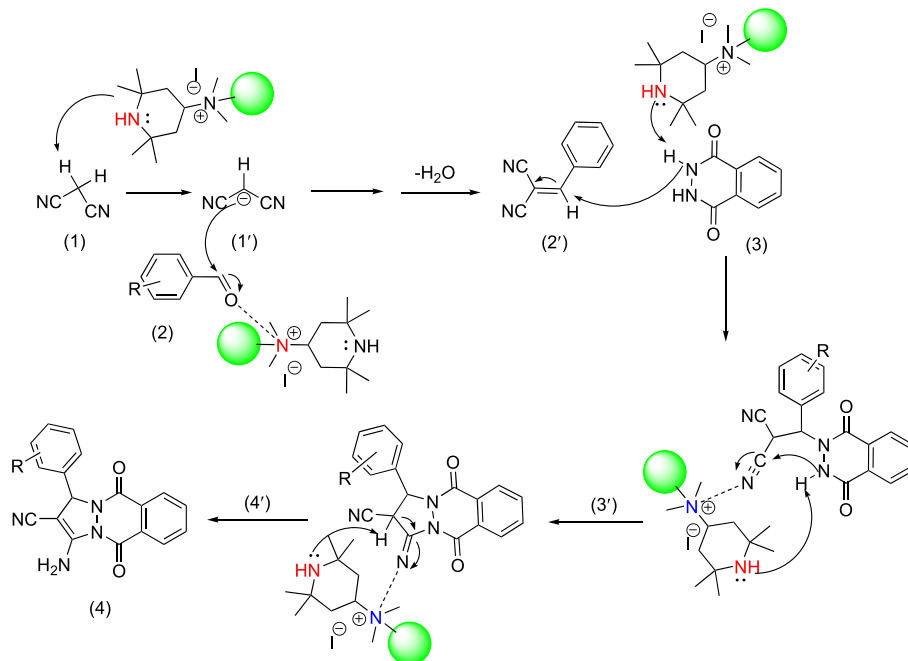
TABLE 3 The comparison of ionic liquid-based hybrid nanocatalyst with other catalysts described in the literature for synthesis of 3-amino-1-aryl-5,10-dioxo-1*H*-pyrazolo[1,2-*b*]phthalazine-2-carbonitrile derivatives via three-component condensation reaction^a

Entry	Catalyst	Condition	Time (min)	Yield (%) ^b	Reference
1	STA–amine–Si-MNPs (10 mg)	CH ₃ OH (reflux)	27	96	[35]
2	Fe _{3-x} Ti _x O ₄ @SiO ₂ @urea MNPs (30 mg)	Solvent-free (100°C)	10	96	[34]
3	2–1'-Methylimidazolium-3-yl-1-ethyl sulfate (0.05% mol)	[Bpy]BF ₄ (70°C)	120	89	[37]
4	PTSA	[bmim]Br (100°C)	168	91	[39]
5	Et ₃ N (20% mol)	EtOH (50°C), MW	60	96	[36]
6	No catalyst	Glycerol (80°C)	50	94	[40]
7	CuFe ₂ O ₄ @SiO ₂ @C ₃ -Imid-C ₄ SO ₃ -PW (60 mg)	Solvent-free (120°C)	10	95	[41]
8	CAN (5% mol)	PEG 400 (100°C)	50	90	[42]
9	NaHCO ₃	Solvent-free (120°C)	30	98	[43]
10	PbO nanoparticles (5% mol)	Solvent-free (80°C)	15	82	[15]
11	Nano-NiFe₂O₄@TiO₂-ILPip (20)	PEG 400 (90°C)	10	97	Present work

Note. The presented work in the article is highlighted in bold format.

^aReaction conditions: malononitrile, phthalhydrazide, 4-chlorobenzaldehyde and catalyst.

^bisolated yield.



SCHEME 4 The plausible mechanism for synthesis of 3-amino-1-aryl-5,10-dioxo-1*H*-pyrazolo[1,2-*b*]phthalazine-2-carbonitriles in the presence of nano-NiFe₂O₄@TiO₂-ILPip particles as a hybrid catalyst

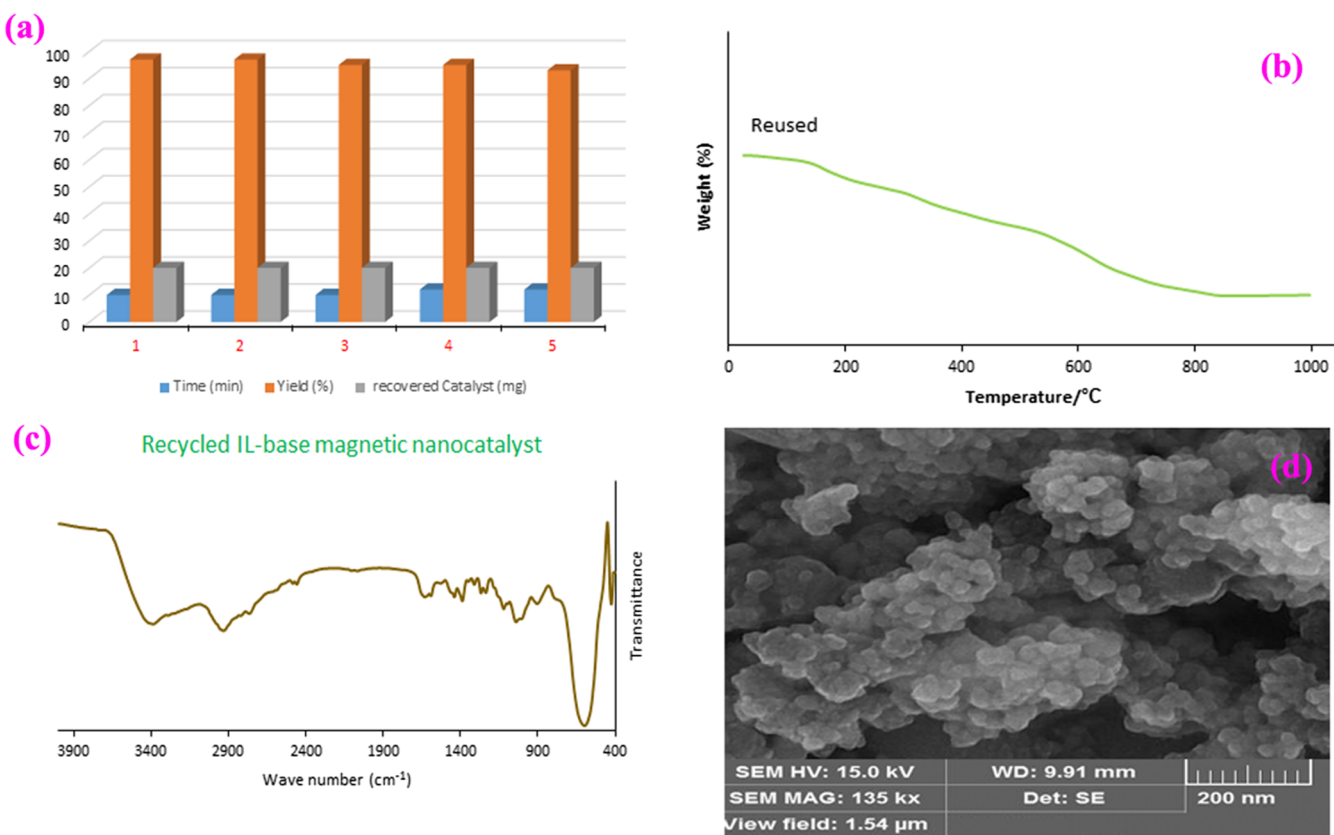


FIGURE 10 (a) The recycling experiment diagram, (b) TGA curve, (c) FT-IR spectrum and (d) FE-SEM image of recycled nano-NiFe₂O₄@TiO₂-ILPip catalyst after five runs

three-component reaction of malononitrile (1.5 mmol), phthalhydrazide (1 mmol) and 4-chlorobenzaldehyde (1 mmol) in the presence of nano-NiFe₂O₄@TiO₂-ILPip catalyst (20 mg) was evaluated. After completion of the reaction, the nanocatalyst was easily separated using an external magnet, washed with EtOH and double-distilled water, and then dried. Experiments revealed almost the same catalytic activity of recycled nanocatalyst without significant loss of activity. As can be seen, the TGA curve (Figure 10b), FT-IR spectrum (Figure 10c) and FE-SEM image (Figure 10d) of the nanocatalyst after five runs confirmed its structure stability and no change in size and morphology was observed.

3 | CONCLUSIONS

A novel and efficient bifunctional IL-based magnetically separable hybrid nanomaterial was prepared and characterized. The prepared hybrid catalyst revealed good catalytic activity in the synthesis of some vital 1*H*-pyrazolo[1,2-*b*]phthalazine-2-carbonitrile derivatives. The hybrid catalyst (NiFe₂O₄@TiO₂-ILPip) could be reused five times without a significant decrease in its catalytic activity. The high isolated yield of pure products, good thermal and chemical stability of nanocatalyst, easy

separation of hybrid catalyst with an external magnet, catalyst reusability without considerable loss of its performance and green reaction conditions are the main and remarkable advantages of the described protocol.

3.1 | Experimental section

3.1.1 | Chemicals and apparatus

All chemicals were purchased from Merck or Fluka Chemical Company and used without further purification. Melting points were measured using capillary tubes on an electrothermal digital apparatus and all products were identified by comparison of their melting points and spectral data with those reported in the literature. Thin-layer chromatography was performed on UV-active aluminum-backed plates of silica gel. FT-IR spectra were recorded on a Bruker Alpha spectrophotometer in the region 400–4000 cm⁻¹ using pressed KBr disks. ¹H and ¹³C-NMR spectra were recorded on a Brucker Avance spectrometer operating at 300 and 75 MHz for ¹H and ¹³C-NMR, respectively, in DMSO-*d*₆ with TMS as an internal standard. X-ray diffraction was performed on a Philips PW1730 Cu-K α radiation of wavelength 1.54 Å. Thermal gravimetric analysis data for nano-

$\text{NiFe}_2\text{O}_4@\text{TiO}_2$ -ILPip were recorded on a Netzsch Proteus System under an N_2 atmosphere at a heating rate of $10^\circ\text{C min}^{-1}$. The FE-SEM and EDS measurement were carried out by a Mira III TESCAN-XMU. The hysteresis loop was measured at room temperature using a vibrating sample magnetometer (model 7300 VSM system, Lake Shore Cryotronic Inc., Westerville, OH, USA). The N_2 adsorption–desorption (BET) was analyzed by SIBATA apparatus, 1100-SA with adsorption of nitrogen at 77 K.

3.1.2 | Preparation of the nano- $\text{NiFe}_2\text{O}_4@\text{TiO}_2$ -PrCl

These nanoparticles were synthesized based on our previously reported procedure.^[15]

3.1.3 | Preparation of the nano- $\text{NiFe}_2\text{O}_4@\text{TiO}_2$ -4-APip

A 1 g aliquot of $\text{NiFe}_2\text{O}_4@\text{TiO}_2$ -PrCl was dispersed in dry toluene (30 ml) for 45 min. Then 10 mmol 2,2,6,6-tetramethyl-4-amino piperidine (0.86 ml) was added to this suspension. The mixture was refluxed for 24 h. The nano- $\text{NiFe}_2\text{O}_4@\text{TiO}_2$ -Pr-Pip-4-amine was isolated using an external magnet, rinsed with dry toluene (3×10 ml) and dried at 80°C .

3.1.4 | Preparation of the nano- $\text{NiFe}_2\text{O}_4@\text{TiO}_2$ -ILPip

A 1 g aliquot of $\text{NiFe}_2\text{O}_4@\text{TiO}_2$ -4-APip was dispersed in dried toluene (30 ml) for 45 min. Then 10 mmol methyl iodide (1 ml) was added to the suspension. The mixture was mixed for 24 h. The MNPs@ TiO_2 -ILPip was isolated by external magnet and rinsed with dry toluene (3×10 ml) and dried at 80°C .

3.1.5 | General procedure for the synthesis of 3-amino-1-aryl-5,10-dioxo-1*H*-pyrazolo[1,2-*b*]phthalazine-2-carbonitriles

A mixture of malononitrile (0.1 g, 1.5 mmol), phthalhydrazide (0.18 g, 1 mmol), aldehyde (1 mmol), and nanocatalyst (20 mg) was heated at 80°C , in PEG400 (5 ml) as a solvent. The reaction progress was followed using thin-layer chromatography technique. After cooling, PEG400 was removed by distilled water (3×10 ml) and the catalyst separated easily by an external magnet. The products were recrystallized in ethanol.

3.1.6 | Selected spectroscopic and physical and data of products

3-Amino-1-(3-nitrophenyl)-5,10-dioxo-5,10-dihydro-1*H*-pyrazolo[1,2-*b*]phthalazine-2-carbonitrile (4a)

Yellow powder; IR (KBr) (ν_{\max} , cm^{-1}): 3364, 3244, 3193, 3030, 2199, 1685, 1664, 1604, 1562, 1443, 1373; δ_{H} (300 MHz, DMSO-*d*₆) 6.16 (1H, s, CH), 7.47–8.24 (10H, m, ArH and NH₂); δ_{C} (75 MHz, DMSO-*d*₆) 60.7, 62.5, 116.4, 122.3, 123.8, 127.1, 127.7, 128.9, 129.5, 130.6, 134.2, 135.0, 141.2, 148.4, 151.5, 154.3, 157.2.

3-Amino-1-(4-hydroxy-3-nitrophenyl)-5,10-dioxo-5,10-dihydro-1*H*-pyrazolo[1,2-*b*]phthalazine-2-carbonitrile (4c)

Light brown powder; IR (KBr) (ν_{\max} , cm^{-1}): 3357, 3295, 3186, 3033, 2200, 1664, 1630, 1570, 1436, 1377; δ_{H} (300 MHz, DMSO-*d*₆) 5.99 (1H, s, CH), 6.92–8.05 (9H, m, ArH and NH₂), 10.93 (1H, s, OH); δ_{C} (75 MHz, DMSO-*d*₆) 60.7, 62.3, 116.4, 119.7, 124.5, 127.1, 127.6, 129.0, 129.3, 129.8, 134.18, 134.3, 135.0, 137.2, 151.3, 152.3, 157.1.

3-Amino-1-(2-chlorophenyl)-5,10-dioxo-5,10-dihydro-1*H*-pyrazolo[1,2-*b*]phthalazine-2-carbonitrile (4e)

Yellow powder; IR (KBr) (ν_{\max} , cm^{-1}): 3372, 3235, 3175, 3025, 2209, 1683, 1659, 1567, 1437, 1382; δ_{H} (300 MHz, DMSO-*d*₆) 6.27 (1H, s, CH), 7.03–8.08 (10H, m, ArH and NH₂); Anal. calcd for $\text{C}_{18}\text{H}_{11}\text{ClN}_4\text{O}_2$: C, 61.64; H, 3.16; Cl, 10.11; N, 15.97; found: C, 61.71; H, 3.21; Cl, 10.15; N, 16.05.

3-Amino-1-(2,4-dichlorophenyl)-5,10-dioxo-5,10-dihydro-1*H*-pyrazolo[1,2-*b*]phthalazine-2-carbonitrile (4h)

Yellow powder; IR (KBr) (ν_{\max} , cm^{-1}): 3371, 3305, 3262, 3192, 3030, 2197, 1658, 1563, 1437, 1381; δ_{H} (300 MHz, DMSO-*d*₆) 6.25 (1H, s, CH), 6.25–8.07 (9H, m, ArH and NH₂); δ_{C} (75 MHz, DMSO-*d*₆) 59.7, 70.2, 116.0, 125.5, 127.1, 127.8, 128.4, 128.7, 129.2, 122.6, 132.7, 132.9, 134.0, 134.3, 135.2, 151.7, 154.0, 157.1.

3-Amino-1-(3,4-dimethoxyphenyl)-5,10-dioxo-5,10-dihydro-1*H*-pyrazolo[1,2-*b*]phthalazine-2-carbonitrile (4m)

Yellow powder; IR (KBr) (ν_{\max} , cm^{-1}): 3370, 3292, 3262, 3033, 2184, 1658, 1602, 1567, 1437, 1379; δ_{H} (300 MHz, DMSO-*d*₆) 3.55 (6H, s, OCH₃), 5.88 (1H, s, CH), 6.68–8.04 (9H, m, ArH and NH₂); δ_{C} (75 MHz, DMSO-*d*₆) 55.9, 56.1, 61.8, 63.4, 111.2, 111.9, 116.6, 119.9, 126.9, 127.6, 129.2, 131.0, 134.0, 135.05, 149.1, 149.2, 150.9, 154.1, 157.1.

ACKNOWLEDGEMENTS

We clarify that the authors listed on the manuscript are not employed by a government agency that has a primary

function other than research and education. Also, the authors are not submitting this manuscript as an official representative or on behalf of the government. This work was supported by the research council of Arak University. There are no financial conflicts of interest to disclose.

ORCID

Mahdia Hamidinasab  <https://orcid.org/0000-0002-4281-8279>

Mohammad Ali Bodaghifard  <https://orcid.org/0000-0001-9732-4746>

Akbar Mobinikhalevi  <https://orcid.org/0000-0002-9732-7282>

REFERENCES

- [1] M. Behalo, I. Gad El-karim, R. Rafaat, *J. Heterocycl. Chem.* **2017**, *54*, 3591.
- [2] N. Wasfy, A. Aly, M. Behalo, N. Mohamed, *Der Pharma Chem.* **2013**, *5*, 82.
- [3] X. Zhang, Q.-R. Zhang, H.-M. Liu, D.-Q. Xue, X.-Y. Zhang, C.-J. Wang, L.-Y. Ma, N. Zhu, P. He, K.-P. Shao, P.-J. Chen, Y.-F. Gu, X.-S. Zhang, C.-F. Wang, C.-H. Ji, *Artic. Eur. J. Med. Chem.* **2014**, *85*, 235.
- [4] S. Grasso, G. De Sarro, A. De Sarro, N. Micale, M. Zappalà, G. Puja, M. Baraldi, C. De Michelis, *J. Med. Chem.* **2000**, *43*, 2851.
- [5] Da-Ch. Liu, G.-H. Gong, Ch-X. Wei, X.-J. Jin, Zh-Sh. Quan, *Bioorg. Med. Chem. Lett.* **2016**, *26*, 1576.
- [6] B. Glišić, L. Senerovic, P. Comba, H. Wadeppohl, A. Veselinovic, D. R. Milivojevic, M. I. Djuran, J. Nikodinovic-Runic, *J. Inorg. Biochem.* **2016**, *155*, 115.
- [7] P. Sagar Vijay Kumar, L. Suresh, G. V. P. Chandramouli, *J. Saudi Chem. Soc.* **2017**, *21*, 306.
- [8] A. Amoozadeh, S. Golian, S. Rahmani, *RSC Adv.* **2015**, *5*, 45974.
- [9] V. Polshettiwar, T. Asefa, *Synthesis and Applications*, Hoboken, New Jersey: John Wiley & Sons **2013**.
- [10] M. Gawande, R. Luque, R. Zboril, *ChemCatChem* **2014**, *6*, 3312.
- [11] W. Xie, H. Wang, *Renewable Energy* **2020**, *145*, 1709.
- [12] W. Xie, F. Wan, *Chem. Eng. J.* **2019**, *365*, 40.
- [13] W. Xie, X. Zang, *Food Chem.* **2018**, *257*, 15.
- [14] M. A. Bodaghifard, M. Hamidinasab, N. Ahadi, *Curr. Org. Chem.* **2018**, *22*, 234.
- [15] M. Hamidinasab, A. Mobinikhalevi, *ChemistrySelect* **2019**, *4*, 17.
- [16] R. Vekariya, *J. Mol. Liq.* **2017**, *227*, 44.
- [17] M. Vafaeezadeh, Z. Bahrami Dizicheh, M. Mahmoodi Hashemi, *Catal. Commun.* **2013**, *41*, 96.
- [18] W. Cheng, X. Chen, J. Sun, J. Wang, S. Zhang, *Catal. Today* **2013**, *200*, 117.
- [19] R. Hosseinzadeh-Khanmiri, Y. Kamel, Z. Keshvari, A. Mobaraki, G. H. Shahverdizadeh, E. Vessally, M. Babazadeh, *Appl. Organomet. Chem.* **2018**, *32*, 1.
- [20] Z. He, D. Liu, Z. Zhou, P. Wang, *J. Sep. Sci.* **2013**, *36*, 3226.
- [21] H. Sahebi, E. Konoz, A. Ezabadi, *New J. Chem.* **2019**, *43*, 13554.
- [22] J. Fu, H. Zang, Y. Wang, S. Li, T. Chen, X. Liu, *Ind. Eng. Chem. Res.* **2012**, *51*, 6377.
- [23] M. A. Zolfigol, M. Mokhlesi, S. Farahmand, *J. Iran. Chem. Soc.* **2013**, *10*, 577.
- [24] A. Khoraamabadi-Zad, M. Azadmanesh, R. Karamian, M. Asadbegy, M. Akbari, *RSC Adv.* **2014**, *4*, 47721.
- [25] O. S. Zaky, M. A. Selim, M. M. Ebied, K. U. Sadek, *J. Heterocycl. Chem.* **2019**, *19*. <https://doi.org/10.1002/jhet>
- [26] R. Sen, P. Jain, R. Patidar, S. Srivastava, R. Rana, N. Gupta, *Mater. Today* **2015**, *2*, 3750.
- [27] M. Chellappa, U. Anjaneyulu, G. Manivasagam, U. Vijayalakshmi, *Int. J. Nanomed.* **2015**, *10*, 31.
- [28] Z. Li, H. Wang, X. Wei, X. Liu, Y. Yang, W. Jiang, *J. Alloy. Comp.* **2016**, *659*, 240.
- [29] A. Mirabedini, S. M. Mirabedini, A. A. Babalou, S. Pazokifard, *Prog. Org. Coatings* **2011**, *72*, 453.
- [30] D. Kannaiyan, S. T. Kochuveedu, Y. H. Jang, Y. J. Jang, J. Y. Lee, J. Lee, J. Kim, *Polymer* **2010**, *2*, 490.
- [31] H. Kim, D. Kim, B. Kwak, G. Han, M. Um, M. Kang, *Chem. Eng. J.* **2014**, *243*, 272.
- [32] K. Nejati, R. Zabihi, *Chem. Cent. J.* **2012**, *6*, 23.
- [33] K. Petcharoen, A. Sirivat, *Mater. Sci. Eng., B* **2012**, *177*, 421.
- [34] D. Azarifar, O. Badalkhani, Y. Abbasi, M. Hasanabadi, *J. Iran. Chem. Soc.* **2017**, *14*, 403.
- [35] P. Arora, J. K. Rajput, *Appl. Organomet. Chem.* **2018**, *32*, e4001.
- [36] M. R. Nabid, S. J. Tabatabaei Rezaei, R. Ghahremanzadeh, A. Bazgir, *Ultrason. Sonochem.* **2010**, *17*, 159.
- [37] Y. Wan, C. Wang, X. Zhang, J. Shi, S. Huang, G. Liu, L. Chen, L. Zhao, H. Wang, *J. Het. Chem.* **2015**, *51*, E77.
- [38] H. Kefayati, S. Amlashi, R. Kazemi-Rad, *C. R. Chim.* **2014**, *17*, 894.
- [39] R. Ghahremanzadeh, G. Shakibaei, A. Bazgir, *Synlett* **2008**, *2008*, 1129.
- [40] A. Mulik, M. Deshmukh, D. Chandam, P. Patil, S. Jagdale, D. Patil, S. Sangpal, *Der Pharma Chem.* **2013**, *5*, 19.
- [41] N. Hosseininasab, A. Davoodnia, F. Rostami-Charati, A. Khojastehnezhad, *Russ. J. Gen. Chem.* **2017**, *87*, 2436.
- [42] M. Kidwai, R. Chauhan, *J. Heterocycl. Chem.* **2014**, *51*, 1689.
- [43] A. Vafaei, A. Davoodnia, M. Pordel, M. R. Bozorgmehr, *Orient. J. Chem.* **2015**, *31*, 2153.
- [44] N. Azgomi, M. Mokhtary, *J. Mol. Catal. A: Chem.* **2015**, *398*, 58.

How to cite this article: Hamidinasab M, Bodaghifard MA, Mobinikhalevi A. Green synthesis of 1*H*-pyrazolo[1,2-*b*]phthalazine-2-carbonitrile derivatives using a new bifunctional base-ionic liquid hybrid magnetic nanocatalyst. *Appl Organometal Chem.* 2019;e5386. <https://doi.org/10.1002/aoc.5386>